cosmetics

MDPI

Article

Willaertia Lysate: A Hydrobiome-Biosourced Ingredient with Multi-Site Antioxidative and Antiaging Properties

Morgan Dos Santos [1], Julie Rorteau [1], Kilian Laho [1], Hanan Osman-Ponchet [2], Manon Barthe [2], Benjamin Quelard [3], Antoine Carlino [3], Adeline Saha [3] and Sandrine Troussieux [3,*]

[1] LabSkin Creations, 69004 Lyon, France; morgan.dossantos@labskincreations.fr (M.D.S.)
[2] Laboratoires PKDERM, 06130 Grasse, France; hanan.osman.ponchet@pkderm.com (H.O.-P.)
[3] Amoéba, 69680 Chassieu, France
* Correspondence: s.troussieux@amoeba-nature.com

Abstract: Aging is synonymous with the skin becoming increasingly thin and fragile, which is associated with a decrease in epidermal cell layers. Beyond this intrinsic aging process, the skin is continually exposed to environmental stressors such as UV radiation that accelerate aging. To fight the signs of aging, a comprehensive program was implemented in this study to evaluate the efficacy of an innovative ingredient, *Willaertia* lysate, through a multi-scale approach encompassing cellular and advanced 3D skin models. The results show that *Willaertia* lysate, initially sourced from French Alps thermal spring waters, is able to (i) promote cell migration; (ii) improve the quality and abundance of the extracellular matrix in aged skins and in young skins exposed to UV radiation to a similar level to that in unexposed young skins; (iii) decrease tyrosinase activity and melanin content; and (iv) reduce oxidative stress after UV exposure by decreasing exposome markers such as protein carbonylation and lipid peroxidation expression. This complete set of coherent results demonstrates the global protective efficacy of *Willaertia* lysate against the effects of photoaging. This study is the first to report the use of a protozoan lysate as a natural and biosourced postbiotic active ingredient in the fields of cosmetics and dermocosmetics.

Keywords: cosmetics; antiaging; antioxidant; *Willaertia magna* C2c Maky; postbiotic; thermal spring water

Citation: Dos Santos, M.; Rorteau, J.; Laho, K.; Osman-Ponchet, H.; Barthe, M.; Quelard, B.; Carlino, A.; Saha, A.; Troussieux, S. *Willaertia* Lysate: A Hydrobiome-Biosourced Ingredient with Multi-Site Antioxidative and Antiaging Properties. *Cosmetics* **2024**, *11*, 200. https://doi.org/10.3390/cosmetics11060200

Academic Editor: Remo Campiche

Received: 26 September 2024
Revised: 12 November 2024
Accepted: 19 November 2024
Published: 21 November 2024

1. Introduction

With increasing life span, skincare has become an ever-growing sector. As we age, our skin becomes increasingly thin and fragile. The number of epidermal cell layers decreases, as do the size and quantity of dermal fibroblasts. Elastin and collagen fibers, which are essential for maintaining skin structure, fail to assemble properly and become rigid, leading to a loss of elasticity and firmness in the skin. Cells that once played a vital role in synthesis and renewal are now transitioning toward senescence and degradation [1]. Beyond this intrinsic aging process, the skin is continually exposed to environmental stressors that accelerate aging. Among these extrinsic factors, UV radiation is the primary cause of cutaneous aging, known as photoaging [2].

To help maintain youthful and healthy skin over time, the cosmetic industry offers a broad spectrum of antiaging active ingredients with very different modes of action and sourcing. Public demand for improved skin health and beauty products has led to the emergence of a new type of products called cosmeceuticals, which lie at the interface of cosmetics and pharmaceuticals [3]. Cosmeceuticals encompass, for example, vitamins recommended for preventing photoaging, including retinol, which has been the gold standard in antiaging treatments for many years. However, retinol is not always well tolerated [4], despite formulations designed to reduce its toxicity [5]. Moreover, face creams and serums containing more than 0.3% retinol, and body care products containing more

than 0.05% retinol, will be banned from over-the-counter sale in Europe from 2026 onwards, following widespread concern about the potentially dangerous side effects of high retinol concentrations (EU Commission Regulation 2024/996 of 3 April 2024).

More recently, bakuchiol, a meroterpene phenol abundant in the seeds and leaves of the plant *Psoralea corylifolia*, has been used in place of retinol, showing similar effects but with better tolerance even though there is no structural resemblance [4,6]. However, bakuchiol was demonstrated to be allergenic in cosmetics [7]. There is a wide range of other molecules with antiaging and/or antioxidant effects, such as hydroxy acids, growth factors, peptides, microbial compounds, and botanical extracts [3,8–11]. In recent years, biotechnology has emerged as a key driver of innovation, particularly through the development of numerous functional compounds derived from microorganisms such as bacteria, fungi, and algae. These advancements have played a significant role in promoting and facilitating the sustainable growth of the cosmetic industry [12,13]. Microbial fermentation, thus, has great potential in cosmetics, with prebiotics referring to fermentation metabolites, probiotics containing living microorganisms, and postbiotics corresponding to cell lysates or non-viable microorganisms. Pre/pro/postbiotics are usually used to maintain a healthy skin microbiome [14]; however, postbiotics can have antiaging properties due to the selection of skin microbiota linked with the aging phenotype of the skin [15]. Postbiotics are usually members of the *Lactobacillus* genera and/or yeasts such as *Saccharomyces cerevisiae* [16], but to the best of our knowledge, the domain of protozoa has never yet been exploited.

Exploration of the hydrobiome of the thermal waters of Aix-les-Bains (Pr Bodennec, Université Lyon 1, personal communication) has led to the isolation of a microorganism with highly interesting biological properties [17]. Several studies have characterized this organism, deposited with the ATCC under the name *Willaertia magna* C2c Maky (PTA-7824). In particular, this organism demonstrated an absence of pathogenicity in culture experiments that were corroborated by omics analyses [18,19]. This strain is a unicellular microorganism belonging to the Protista kingdom. It is characterized by a deformable cell body emitting shape-changing extensions called pseudopodia, which enable it to capture microscopic prey via phagocytosis. In its natural environment, it is a natural predator and regulator of populations of environmental bacteria and waterborne microorganisms [19]. These kinds of microorganisms, such as *W. magna* C2c Maky, are ubiquitous protozoan that inhabit common aquatic environments [19,20].

A novel natural and biosourced ingredient based on the patented use of a lysate of *W. magna* C2c Maky was developed as a bioactive hydrobiome-derived postbiotic for use in cosmetics and dermocosmetics. The aim of this study was to investigate the intrinsic properties of this *Willaertia* lysate for use in the field of cosmetics, particularly to fight the signs of aging. An initial study identified promising potential properties associated with the stimulation of specific gene expression. These findings were further confirmed through in vitro experiments, including wound healing, skin lightening, and assessments using three-dimensional (3D) reconstructed skin models. These models were used to study both intrinsic and extrinsic aging factors, enabling an evaluation of the effects of this ingredient on a range of established markers within the epidermis, dermal–epidermal junction, and dermis.

2. Materials and Methods

2.1. Expression of Genes of Interest

Target gene induction analysis was performed on human epithelial cells (ATCC CCL-2) cultured in DMEM (Thermo-Fisher Scientific, Waltham, MA, USA) supplemented with fetal calf serum (10%), with penicillin and streptomycin (5000 U/mL and 5000 µg/mL, respectively) at 37 °C and under 5% CO_2 atmosphere in a 6-well plate with a flat bottom.

Cells at a concentration of 1×10^6 cells/well were either stimulated or not stimulated with *Willaertia* lysate lot 22.LY.040 (Amoéba, Chassieu, France) containing 7.79% dry matter (*w*/*v*) after its dilution at 0.2% and 0.1% for 8 h at 37 °C under 5% CO_2 atmosphere.

Total RNA was isolated using Qiagen's RNAeasy protocol, quantified via NanoDrop (260 nm), and normalized to 100 ng/µL (stored at −20 °C). Only samples with a 260/280 ratio above 2 were used for analysis.

The mRNA contained in the total RNA samples was transformed into cDNA via reverse transcription using oligo-dt 18 and then stored at −20 °C. Quantitative PCR was performed on a CFX96 Bio-Rad using the sybergreen method with primers specific to the targeted genes of interest. The results were expressed as the fold change (FC) according to Formula (1) (n = 3, mean ± standard deviation):

$$FC = 2^{-\Delta\Delta Ct} \quad (1)$$

where ΔΔCt = (Ct target gene − Ct constitutive gene)$_{test}$ − (Ct target gene − Ct constitutive gene)$_{control.}$

The constitutive gene was GAPDH and the target genes were TLR2 (immunity), TGF-beta (cell multiplication, anti-inflammation), RunX1 (cell multiplication, tissue cohesion, cell differentiation), PiwiL1 (cell renewal), SGK1 (UV protection, antioxidative stress, photoaging), FOXO1 (UV protection, antioxidative stress, photoaging), BCL2 (anti-cell death), HMMR (hyaluronic acid receptor, cell mobility), HAS (hyaluronic acid synthesis), COL1A1 (collagen synthesis), and FBL5 (wound healing).

2.2. Antioxidant Activity

The antioxidant activity was measured using the 2,2-diphenyl-1-picrylhydrazil (DPPH) method [21–23].

- Amoeba Extracts

Willaertia lysate lot 22-LY-130 (Amoéba, Chassieu, France) containing 10.64% dry weight of the active substance was mixed with methanol at 4 concentrations (1, 5, 10, and 15 mg dry weight/mL). The mixtures were then shaken for 30 s and extracted with ultrasound (45 kHz) for 30 min (Ultrasonic cleaner, USC600-TH—VWR). The mixtures were centrifuged at 10,000× *g* for 15 min. The supernatants were stored at −20 °C until use.

- DPPH Assay

The DPPH reagent (Sigma–Aldrich, Saint Quentin Fallavier, France) was dissolved in methanol to a concentration of 0.1 mM. A volume of 50 µL of *Willaertia* lysate extracts was placed in a microplate (with 96 flat-bottomed wells), and the procedure was performed in triplicate. Then, 200 µL of DPPH at 0.1 mM was added to the wells. As a positive control, 50 µL of ascorbic acid solution mixed with methanol at 4 concentrations ranging from 10 to 25 µg/mL was placed in the microplate, and 200 µL of DPPH was added. As a blank control, 50 µL of methanol was used, and 200 µL of DPPH was added. Finally, the plate was incubated in a microplate reader (Victor® Nivo, PerkinElmer, Villebon-sur-Yvette, France), and the absorbance was recorded every minute at 521 nm for 30 min at room temperature in the dark.

The inhibition percentage (I%) corresponding to the quantity of DPPH radicals reduced by the extract at a given concentration was calculated according to Formula (2):

$$I\% = \left[\frac{AB - AS}{AB}\right] \times 100 \quad (2)$$

where AB is the absorbance of the blank, and AS is the absorbance of the sample.

The inhibitory concentration IC50, which is the concentration of the sample required to eliminate 50% of DPPH free radicals, was also calculated graphically using a linear regression analysis.

The results were expressed as the mean of three independent replicates.

2.3. Dermal Fibroblast and Keratinocyte Cell Migration Measure

- Cell culture

Normal human dermal fibroblasts (NHDFs) in primary culture were seeded with fibroblast basal medium (Innoprot, Derio, Spain), and the human epidermal keratinocyte cell line HaCaT was seeded with DMEM-F12 (VWR, Radnor, PA, USA), both supplemented with 2% fetal bovine serum, 1% fibroblast growth supplement, and 1% penicillin/streptomycin. Cell incubation was conducted in a humidified cell incubator set at 37 °C and 5% CO_2.

- In vitro scratch test

NHDF or HaCaT cells were seeded in Ibidi® 2-well silicone culture inserts (ibidi GmbH, Gräfelfing, Germany) in a 24-well plate. The growth area of each well insert was 0.22 cm^2, the width of the cell-free gap was 500 µm ± 100 µm, the cell density was 70,000 cells per well insert, and the volume of the culture medium was 70 µL per well insert. The NHDF and HaCaT cells were allowed to proliferate until confluency for 24 h in the humidified cell incubator set at 37 °C and 5% CO_2.

The Ibidi culture inserts were then removed, and the cells were exposed to different treatments (500 µL/well of 24-well plate) for 25 h or 50 h, with three replicates per treatment condition (n = 3). The three treatments—the control (untreated group), and the *Willaertia* lysate lot 22.LY.077 (Amoéba, Chassieu, France) containing 9.24% of dry matter (w/v) diluted at 1×10^{-5}% and at 1×10^{-4}%—were compared.

- Image acquisition

The culture plate was placed on a CytoSMART OMNI brightfield device (Axion Biosystems, Atlanta, GA, USA) inside the culture incubator. Photographic images were captured every hour over the culture period using the CytoSMART OMNI brightfield live-cell imager equipped with a high-resolution digital camera

The results were expressed as the closure area and the area under the curve (AUC).

- Statistical analysis

Statistical significance was determined through analysis of variance (ANOVA single factor). Statistically significant differences were indicated by asterisks as follows: * $p < 0.05$, ** $p < 0.01$, and *** $p < 0.001$).

2.4. Murine Melanoma Cell Pigmentation Assays

- Cell culture

Cells from the murine melanoma cell line B16-F10 were cultured in DMEM supplemented with fetal calf serum (10%) and with penicillin and streptomycin (5000 U/mL and 5000 µg/mL, respectively) at 37 °C and under 5% CO_2 atmosphere. The cells were seeded in a 24-well plate at a cell density of 50,000 cells/well and a volume of culture medium of 500 µL per well. The cells were allowed to proliferate until confluency in a humidified cell incubator set at 37 °C and 5% CO_2.

- Tyrosinase enzyme activity and pigmentation assays

B16-F10 cells were exposed to different treatments (500 µL/well of 24-well plate) for 48 h. The different treatment conditions, with three replicates per treatment condition (n = 3), were tested as follows:

- Control (untreated group);
- 3-isobutyl-1-methyl-xanthine (IBMX) at 100 µM (Sigma–Aldrich, Saint Quentin Fallavier, France);
- IBMX + kojic acid at 200 µM (Sigma–Aldrich);
- IBMX + *Willaertia* lysate at 1×10^{-5}%;
- IBMX + *Willaertia* lysate at 1×10^{-4}%;
- IBMX + *Willaertia* lysate at 1×10^{-3}%.

Melanin content was evaluated on BF16-F10 cells lysed in 1N NaOH (200 µL/well of 24-well plate) and incubated at 80 °C for 1 h via optical density measurement at 405 nm.

Tyrosinase enzyme activity was determined on B16-F10 cells lysed in 1% Triton X-100 (100 µL/well of 24-well plate). The cell lysate (20 µL) was incubated with 2 mM of L-DOPA (100 µL) at 37 °C for 1 h, and the kinetics of formation of dopachrome was monitored at 490 nm.

- Statistical analysis

Statistical significance was determined through analysis of variance (ANOVA single factor). Statistically significant differences were indicated by asterisks as follows: * $p < 0.05$, ** $p < 0.01$, and *** $p < 0.001$).

2.5. Aging Studies on Reconstructed Skins

- Ethical considerations and human cutaneous cell isolation

Human skin tissue was collected according to the principles of the Declaration of Helsinki, and its use was declared to the French Research Ministry (declaration no DC-2020-4346). Written informed consent was obtained from the donor according to the French bioethical law of 2014 (loi 94–954 du 29 Juillet 1994). Primary cultures of human fibroblasts, keratinocytes, and melanocytes were established from the healthy skin biopsy obtained from an infant donor (<5 years old) or an adult donor (>40 years old). Normal human epidermal keratinocytes (NHEKs), melanocytes (NHEMs), and dermal fibroblasts (NHDFs) were isolated from human skin, as previously described [24].

- Three-dimensional reconstructed aged skin for intrinsic aging study

Three-dimensional (3D) full-thickness reconstructed skin models were obtained by culturing NHDFs (>40 years old) in a scaffold made of collagen, glycosaminoglycans, and chitosan (LabSkin matriX^{TM}, Lyon, France) for 21 days under optimized cell culture conditions for ECM neo-synthesis, as previously described [25]. NHEKs were then seeded on the top of the dermal equivalent constructs and raised at the air/liquid interface to allow the formation of the epidermal compartment.

From day 10 until the end of the culture period, the 3D reconstructed skin models were treated in a systemic way with *Willaertia* lysate lot 22-LY-040 containing 7.79% dry matter (w/v) diluted at 0.1×10^{-3}%. The treatments were renewed at every medium renewal each week. Skin equivalent samples harvested on day 42 of total cell culture were immediately fixed in 4% neutral-buffered formalin (Diapath) for 24 h and then embedded in paraffin or in an optimal cutting temperature (OCT) compound and frozen at −80 °C for histological and immunohistological analysis, respectively. For each cell culture condition and analysis, 3D skin equivalents were produced in triplicate.

- Three-dimensional reconstructed young skin for extrinsic aging study

Three-dimensional full-thickness reconstructed skin models were obtained by culturing NHDFs (<5 years old) in a scaffold made of collagen, glycosaminoglycans, and chitosan (LabSkin matriX^{TM}) for 21 days under optimized cell culture conditions for ECM neo-synthesis as previously described [25]. NHEKs and NHEMs were then seeded on the top of the dermal equivalent constructs and raised at the air/liquid interface to allow the formation of the epidermal pigmented compartment. For each cell culture condition and analysis, 3D skin equivalents were produced in triplicate.

From day 10 until the end of the culture period, the 3D reconstructed skin models were treated in a systemic way with *Willaertia* lysate diluted at 0.2×10^{-3}%. The treatments were renewed at every medium renewal each week. On day 40, the tissue constructs were exposed to 100 mJ/cm^2 UVB with UV Stratalinker® 1800 (Stratagene, La Jolla, CA, USA). Skin equivalent samples harvested on day 42 of total cell culture were immediately fixed in 4% neutral-buffered formalin (Diapath, Martinengo, Italy) for 24 h and then embedded in paraffin or in an optimal cutting temperature (OCT) compound and frozen at −80 °C for histological and immunohistological analysis, respectively.

- Histological analysis

To evaluate the global cutaneous structure of the samples, hematoxylin phloxine saffron (HPS) staining was performed. For each condition, paraffin sections of 5 µm were cut. After dewaxing and rehydration, the samples were stained with HPS. After rinsing, the samples were dehydrated before being mounted on slides using a hydrophobic mounting medium.

- Immuno-histological analysis

To detect immunofluorescence on the paraffin sections, after the heat-mediated antigen retrieval treatment, non-specific binding was blocked in PBS containing 4% BSA. The sections were then incubated with the primary antibodies of interest diluted in PBS containing 4% BSA overnight at room temperature.

After incubation for 1 h with an AlexaFluor-568-conjugated anti-mouse/rabbit secondary antibody (Molecular Probes, Thermo Fisher Scientific, Waltham, MA, USA), nuclear counterstaining using DAPI was carried out routinely. As a negative control, the primary antibody was replaced by the corresponding IgG class.

For immunohistochemistry on the paraffin sections, after the heat-mediated antigen retrieval treatment, non-specific binding was blocked in PBS containing 4% BSA. The sections were then incubated with the primary antibodies of interest diluted in PBS containing 4% BSA overnight at room temperature. The studied markers were the following:

- Ki67, loricrin, and filaggrin for epidermis;
- Collagen-7 for the dermal–epidermal junction (DEJ);
- Hyaluronic acid for dermis.
- Malonyl dialdehyde (MDA) and carbonylation for antioxidative stress

After incubation for 1 h with EnVision anti-mouse/rabbit-HRP secondary antibody (Dako EnVision+, HRP) and applying DAB+ substrate solution to the sections, the color of the antibody staining was revealed. The slides were counterstained by immersing them in a 25% Harris hematoxylin counterstaining solution. As a negative control, the primary antibody was replaced by the corresponding IgG class.

- Image acquisition and analysis

The specimens stained in HPS were observed using an Axio Observer A1/D1 optical microscope, and images were captured using AxioCam HRc and ZEN 2 pro (Carl Zeiss SAS, Marly-le-Roi, France). Sixteen-bit images were saved in an uncompressed tagged image file format (tiff). Nine representative images were captured for each condition in the same manner. The immunostained specimens were observed using a Zeiss Axio Observer D1 microscope. Sixteen-bit images were saved. Three representative images were captured for each condition in the same manner (n = 9 in total).

For the markers of interest, positive red-stained tissue areas were automatically detected. The surface area of interest was measured automatically. The data were normalized based on the dermal–epidermal junction length for dermal–epidermal markers and based on the dermal area for dermal markers (for example loricrin/DEJ length).

The data were expressed in percentage of density.

Statistical analysis was performed with R (R Foundation for Statistical Computing, Vienna, Austria), and normality was checked using the Shapiro–Wilk normality test. The normal distribution led to a parametric test. Analysis of variance was performed using an ANOVA test, then the conditions were compared with each other using pairwise *t*-tests as post-hoc tests. The absence of a normal distribution led to a non-parametric test. Analysis of variance was therefore performed using a non-parametric Kruskal–Wallis test, and then the conditions were compared with each other using a non-parametric Wilcoxon–Mann–Whitney test as post hoc tests.

For all data, statistical significance was assessed via a one-way Student's *t*-test, and statistically significant differences were indicated by asterisks as follows: * $p < 0.05$, ** $p < 0.01$, and *** $p < 0.001$.

3. Results

3.1. Preliminary Test to Evaluate the Potential Activity of Willaertia Lysate

Willaertia lysate at two dilutions was tested to evaluate its potential activity on 11 genes involved in the cellular repair process (Table 1).

Table 1. Targeted genes and their function.

Gene Name	Function	References
TLR2	Immunity	[26–28]
TGF-beta	Cellular multiplication, anti-inflammation	[29,30]
RunX1	Cell regeneration regulation, cellular multiplication, cell cohesion, and differentiation	[31–33]
PiwiL1	Cell renewal	[34,35]
SGK1	Blood pressure regulation, UV protection, oxidative stress, cell survival	[36–38]
FOXO1	Stress resistance, antioxidation	[39–42]
BCL2	Regulation of apoptosis	[43–45]
HMMR	Hyaluronic acid receptor, neoplastic process	[46]
COL1A1	Collagen synthesis	[47]
HAS	Hyaluronic acid synthesis	[48–50]
FBL5	Wound healing	[51–53]

A moderate stimulation (1.5- to 1.99-fold increase) was observed in genes related to wound healing (FBL5) and hyaluronic acid synthesis (HAS) at a 0.2% dilution of *Willaertia* lysate (1.6×10^{-2}% dry weight), and a strong stimulation (≥2-fold increase) was noted for genes associated with anti-apoptosis (BCL2), cellular renewal (PIWI1L), UV protection, and antioxidative stress (FOXO1 and SGK1), with maximum expression observed at a 0.2% dilution, whereas the highest expression of the BCL2 gene was achieved with a 0.1% dilution of *Willaertia* lysate (Figure 1).

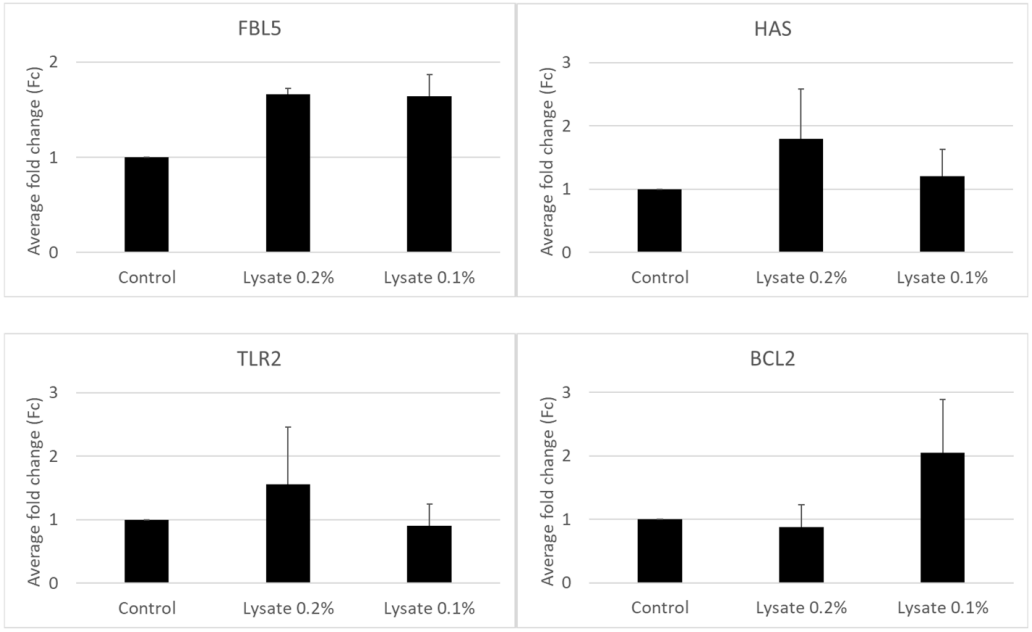

Figure 1. *Cont.*

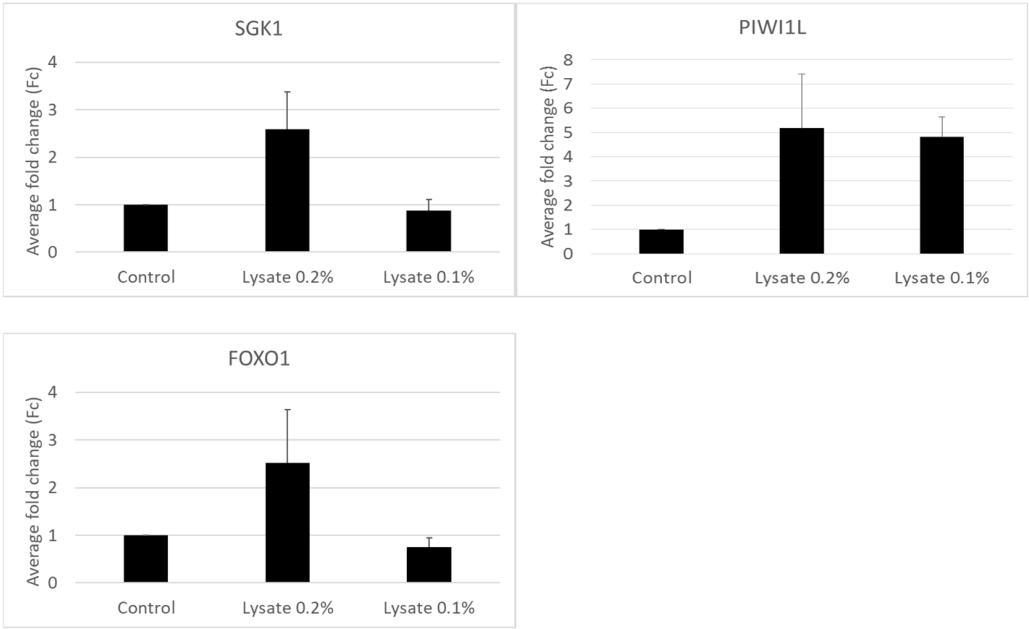

Figure 1. Average fold change in the expression of overexpressed targeted genes.

Therefore, *Willaertia* lysate showed significant potential in enhancing cellular functions linked to aging, including cell protection, cell renewal, UV protection, and antioxidative stress. The findings support the potential efficacy of *Willaertia* lysate in promoting cellular health and longevity.

3.2. Wound Healing Assay

Considering the overexpressed genes, the potential of *Willaertia* lysate in promoting cell migration was evaluated via a scratch test on human dermal fibroblast cells and the human keratinocyte cell line.

Regarding the control curve, the wound closure area increases gradually over time, indicating the occurrence of basal cell migration and natural wound healing processes (Figure 2). NHDF cells treated with 10^{-4}% of *Willaertia* lysate (9.2×10^{-6}% dry weight) exhibit a higher wound closure area compared to the control and the 10^{-5} treated cells (Figure 2). This result demonstrates the dose-dependent efficacy of the lysate in promoting cell migration, thereby improving the wound-healing process.

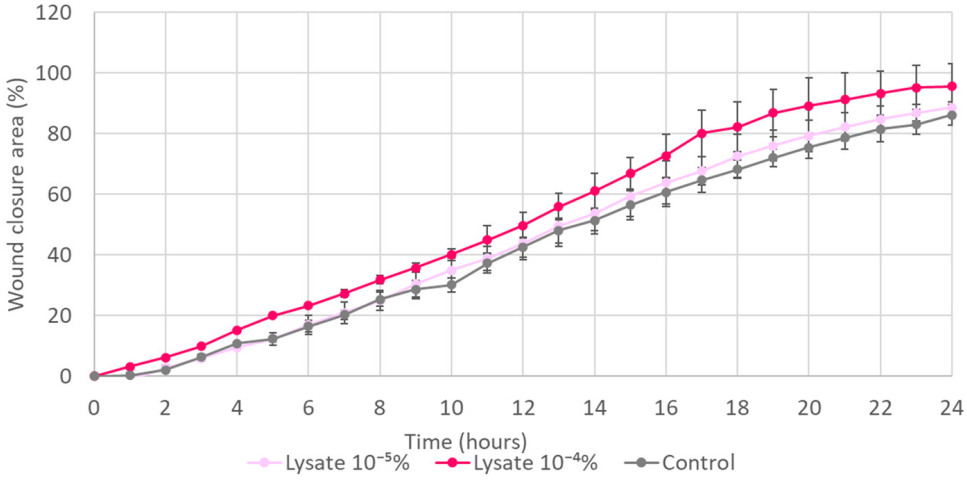

Figure 2. Wound closure area of human dermal fibroblasts treated with two dilutions of *Willaertia* lysate. Results are expressed as mean ± SD (n = 3 biological replicates).

The area under the curve (AUC) is a measure of the total extent of cell migration over time. The treatment of NHDF cells with *Willaertia* lysate solution (10^{-4}% dilution) increased the AUC significantly by 20% ($p < 0.05$) compared to the control group under normal culture conditions, suggesting that it promoted cell migration in a dose-dependent manner (Figure 3).

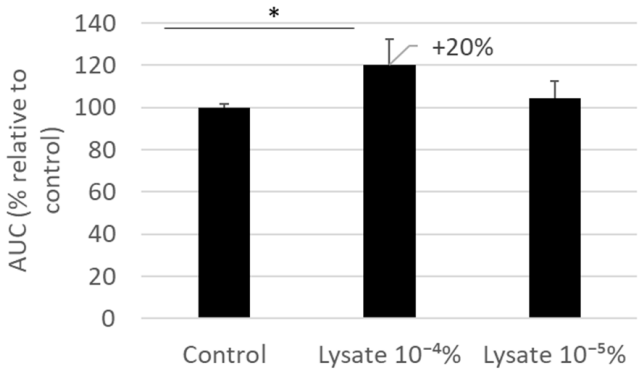

Figure 3. The area under the curve of the closure area of human dermal fibroblasts was treated with two dilutions of *Willaertia* lysate. Results are expressed as mean ± SD (n = 3 biological replicates), * $p < 0.05$.

On human keratinocytes (HaCat cells), the treatment with 10^{-4}% *Willaertia* lysate resulted in an increase in the AUC by +14% compared to the control group. This difference was visualized through image acquisition (Figure 4).

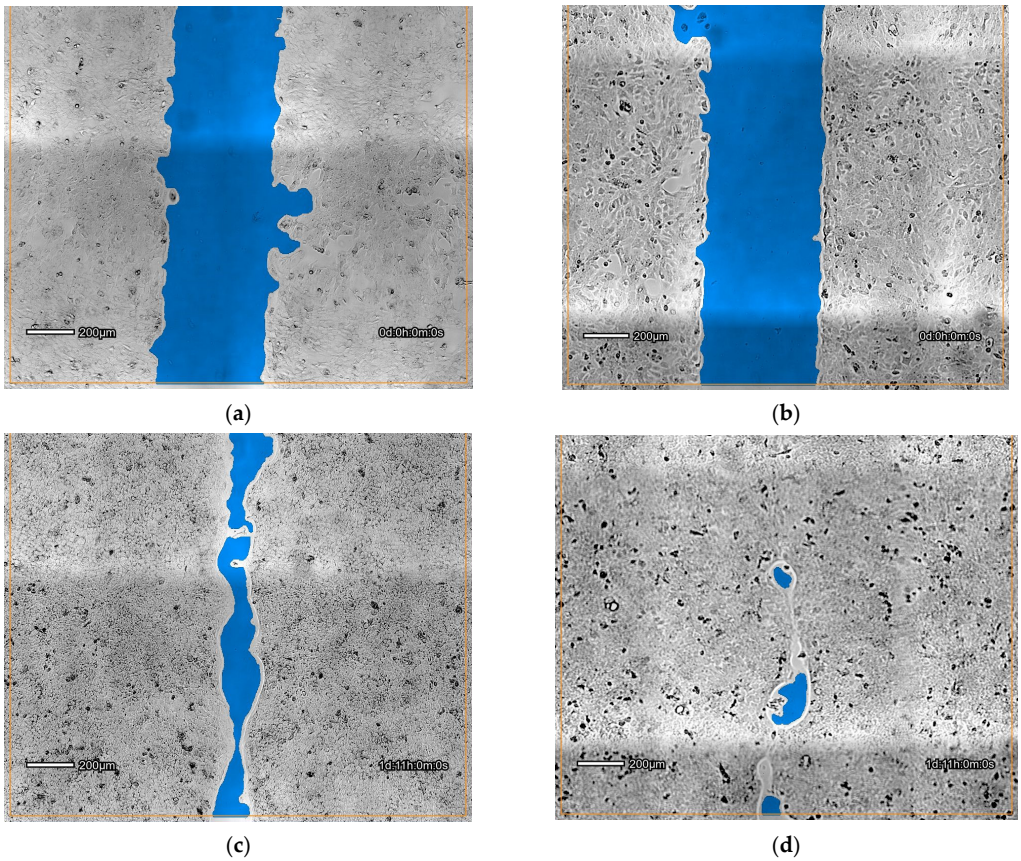

Figure 4. Images of HaCat cell migration: (**a**) at T0 without treatment; (**b**) at T0 with *Willaertia* lysate diluted at 10^{-4}%; (**c**) after 35 h of culturing without treatment; and (**d**) after 35 h of culturing with *Willaertia* lysate diluted at 10^{-4}%. The blue color indicates the cell-free scratch area.

These results demonstrate that *Willaertia* lysate promotes cell migration in both keratinocyte and fibroblast cell types.

3.3. Pigmentation Assay

The objective of this assay was to evaluate the potential effect of *Willaertia* lysate on pigmentation using the B16-F10 murine melanoma cell line, both by measuring its capacity to decrease tyrosinase enzyme activity and melanin content.

3.3.1. Tyrosinase Activity

Tyrosinase activity increased significantly by 49% in the presence of IBMX, known to stimulate pigmentation mechanism, compared to the control group. This increase was significantly reduced by 15% with the addition of kojic acid, known to inhibit tyrosinase activity, and by 7%, 11%, and 9% with treatment with *Willaertia* lysate diluted at 10^{-5}%, 10^{-4}%, and 10^{-3}%, respectively (Figure 5). These data suggest that *Willaertia* lysate inhibited the tyrosinase activity in B16-F10 melanocytes when used between 10^{-5}% and 10^{-3}%. It is worth noticing that, at 10^{-4}% dilution, the decrease in tyrosinase activity was not significantly different from that under the kojic acid condition ($p = 0.1$), meaning that the efficacy of the *Willaertia* lysate at this concentration was as good as the effect of kojic acid.

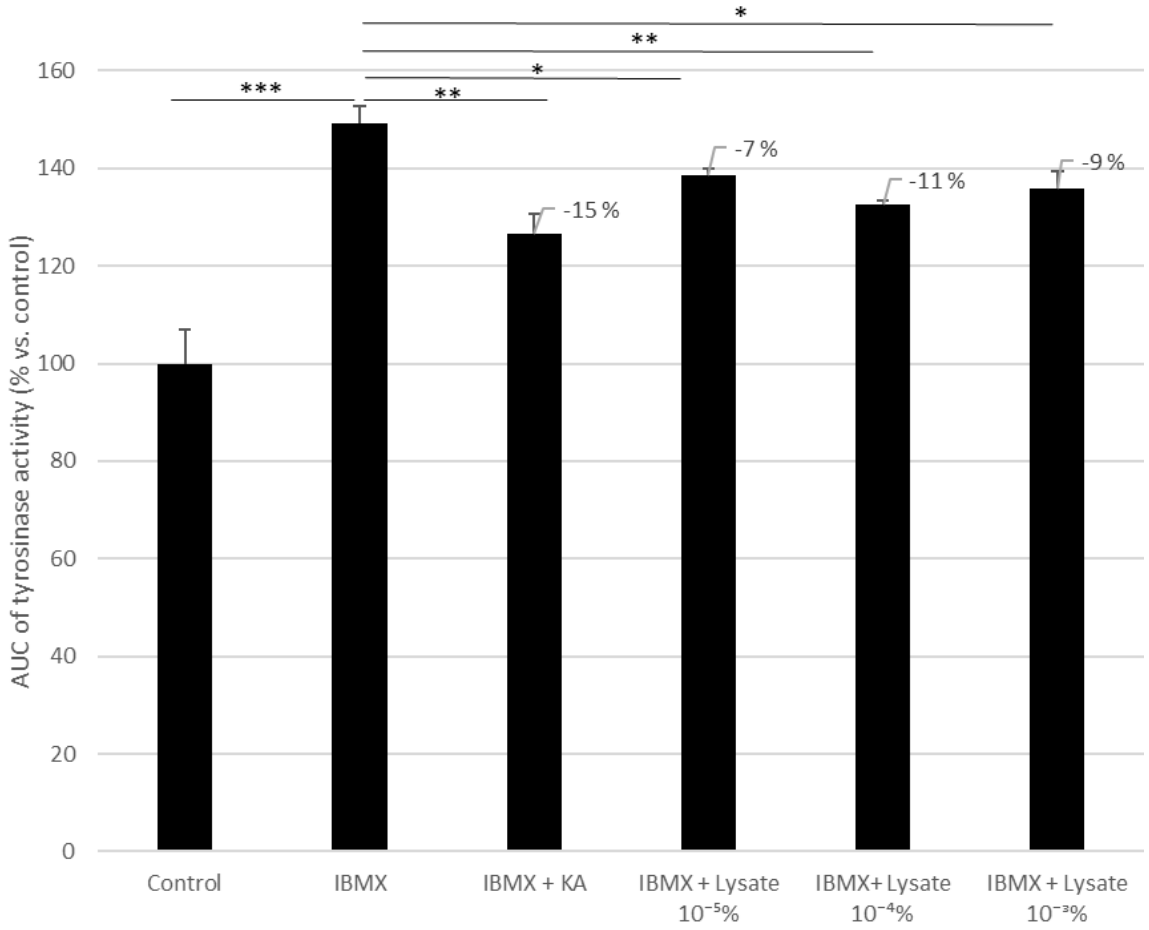

Figure 5. Area under the curve of tyrosinase activity of B16-F10 melanocytes treated with IBMX, IBMX + kojic acid (KA), and three dilutions of *Willaertia* lysate (10^{-5}%, 10^{-4}%, and 10^{-3}%). Results are expressed as mean ± SD (n = 3 biological replicates), * $p < 0.05$, ** $p < 0.01$, *** $p < 0.001$.

3.3.2. Melanin Synthesis

In B16-F10 cells treated with IBMX and kojic acid, the melanin content decreased significantly by 24% (Figure 6) compared to the IBMX group ($p < 0.001$). This confirmed the effect of kojic acid on melanin synthesis, thereby validating the pigmentation assay as kojic acid represented the positive control. These results clearly show that *Willaertia* lysate induced a concentration-dependent decrease in melanin synthesis in B16-F10 melanocytes. It significantly decreased the melanin content by 12% ($p < 0.05$) and 22% ($p < 0.01$) at 10^{-4}% and 10^{-3}% dilutions, respectively.

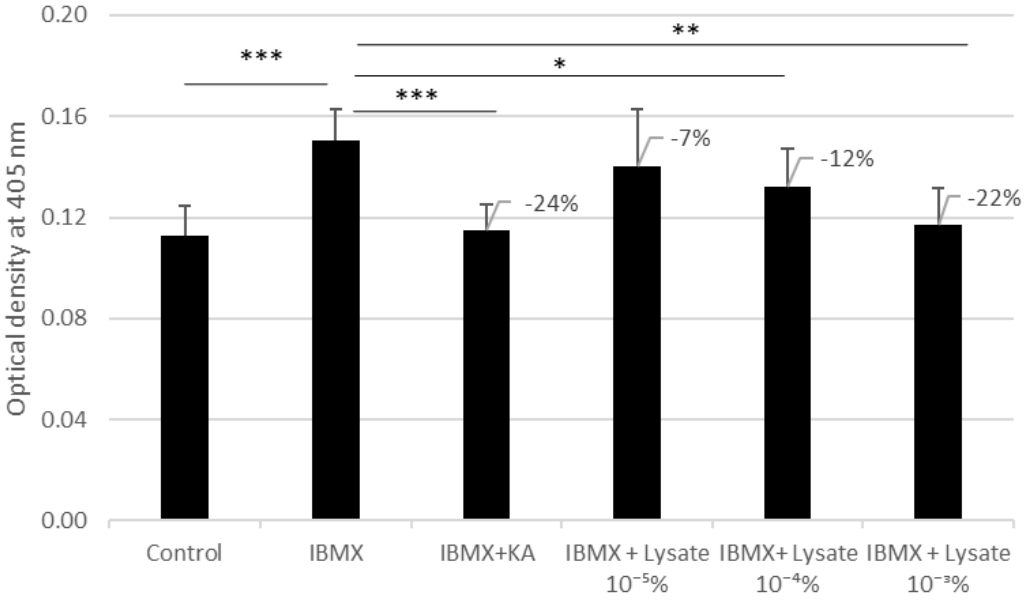

Figure 6. Concentration of melanin in B16-F10 melanocytes treated with IBMX, IBMX + kojic acid (KA), and three dilutions of *Willaertia* lysate (10^{-5}%, 10^{-4}%, and 10^{-3}%). Results are expressed as mean ± SD (n = 3 biological replicates), * $p < 0.05$, ** $p < 0.01$, *** $p < 0.001$.

The treatment of murine melanoma B16-F10 cells with *Willaertia* lysate showed a concentration-dependent decrease in both tyrosinase activity and melanin content. These two combined effects indicated that *Willaertia* lysate was effective in reducing pigmentation.

3.4. Intrinsic Aging Study

The objective of this investigation was to evaluate the effects of *Willaertia* lysate on the histological characteristics of 3D reconstructed aged skin models, more precisely on different specific cutaneous markers using immunohistological techniques.

3.4.1. Histological Analysis of 3D Young vs. 3D Aged Untreated and Treated Skin Models

The global structure of the reconstructed aged skin model was consistent at both the epidermal and dermal levels, showing a pluristratified epidermis that was well differentiated from the basal layer to the *stratum corneum*, and well anchored on top of the dermal equivalent filled with fibroblasts and a neosynthesized extracellular matrix (ECM). The dermal–epidermal junction (DEJ) seemed cohesive and regular. However, compared with the young condition (Figure 7a), aging had an impact on both dermal and epidermal compartments. The extracellular matrix was less dense and abundant, and it was disorganized, impacting tissue elasticity and hydration. The epidermal thickness decreased with fewer layers of living cells. Moreover, the terminal differentiation was disrupted, with thinner *stratum granulosum* and *stratum corneum*, thereby impacting barrier function (Figure 7b).

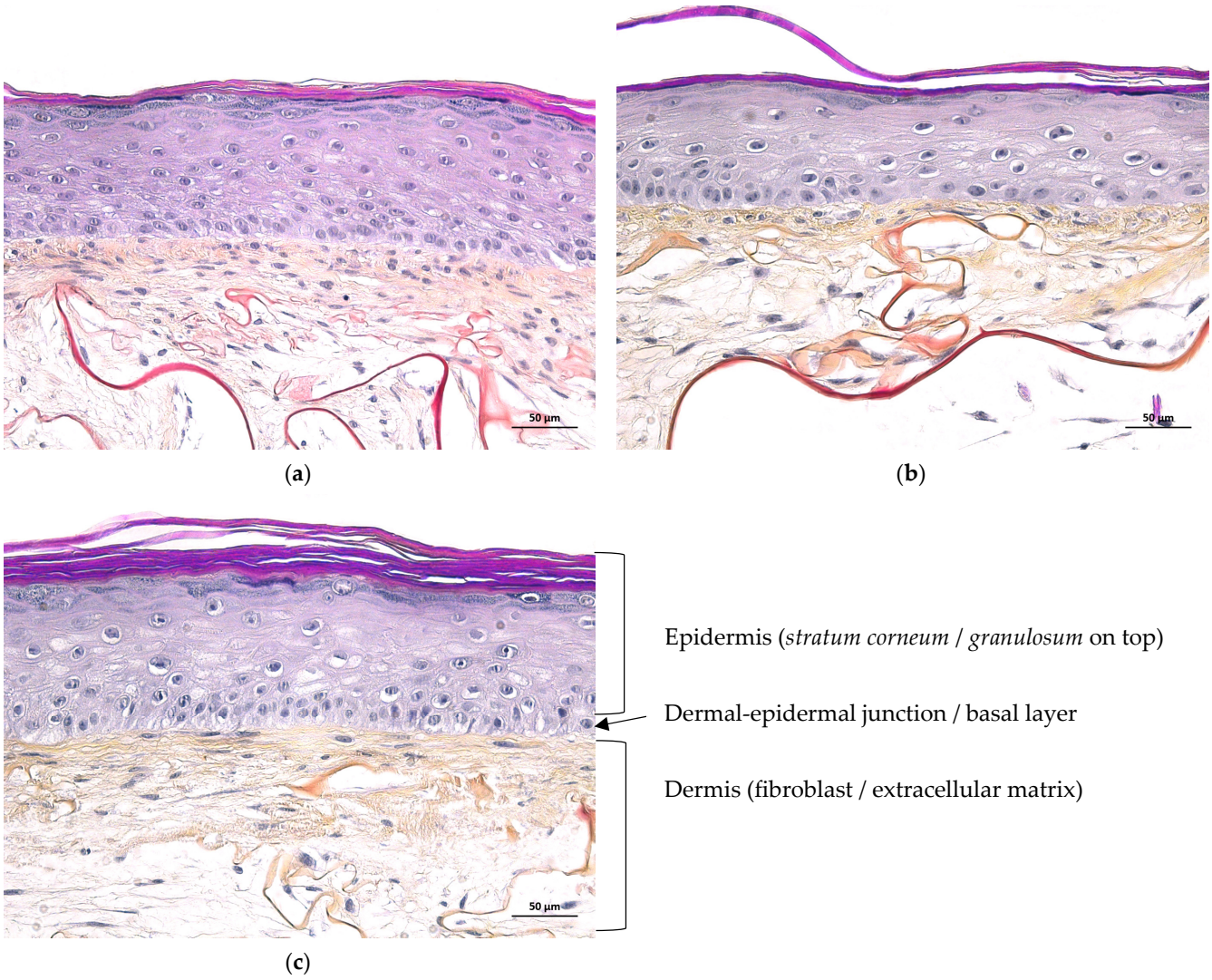

Figure 7. Histological analysis of 3D reconstructed skins: (**a**) untreated young skin; (**b**) untreated aged skin; and (**c**) aged skin treated with *Willaertia* lysate diluted at 0.1×10^{-3}%.

The histological observations showed some beneficial effects of *Willaertia* lysate on the 3D reconstructed aged skin model. Compared with the untreated aged condition, the treatment with *Willaertia* lysate diluted at 0.1×10^{-3}% (7.8×10^{-6}% dry weight) increased the epidermal thickness. Moreover, there was a recovery of terminal differentiation after the treatment compared with the untreated condition. Concerning the dermal compartment, the *Willaertia* lysate treatment improved the quality and abundance of the ECM (Figure 7c).

3.4.2. Immuno-Histological Analysis of Specific Markers in 3D Young Untreated vs. 3D Aged Untreated and Treated Skin Models

To gain a deeper understanding of these effects, further investigations were carried out to decipher more precisely the cellular mechanisms underlying the effects of *Willaertia* lysate at both the epidermal and dermal levels. To conduct such investigations and confirm the histological observations, different cutaneous markers were selected to be explored by means of immuno-histological analysis. The selected markers were Ki67 (Figure 8a), filaggrin (Figure 8b), and loricrin (Figure 8c) for the epidermis; collagen-7 (COL VII) (Figure 8d) for the dermo-epidermal junction (DEJ); and hyaluronic acid (HA) for the dermis (Figure 8e).

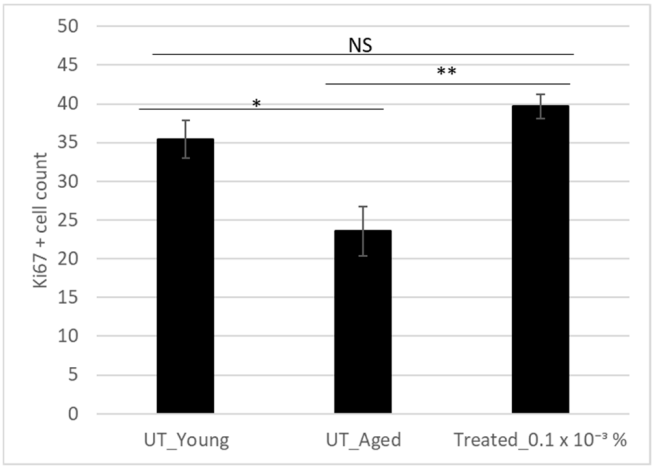

(**a**)

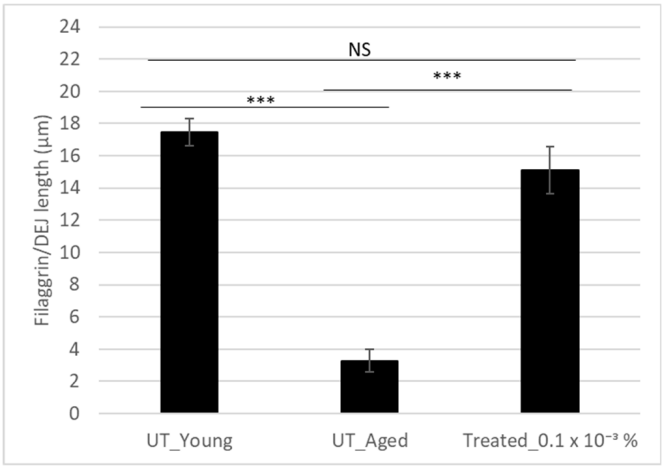

(**b**)

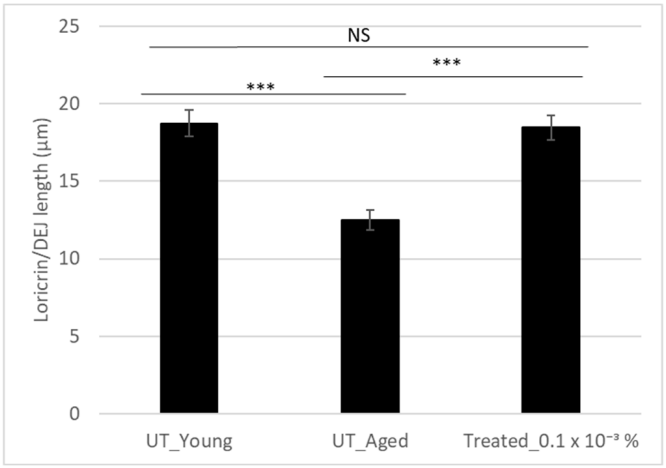

(**c**)

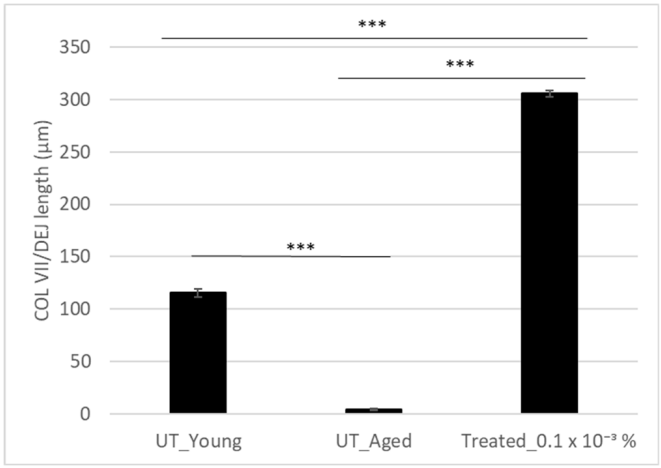

(**d**)

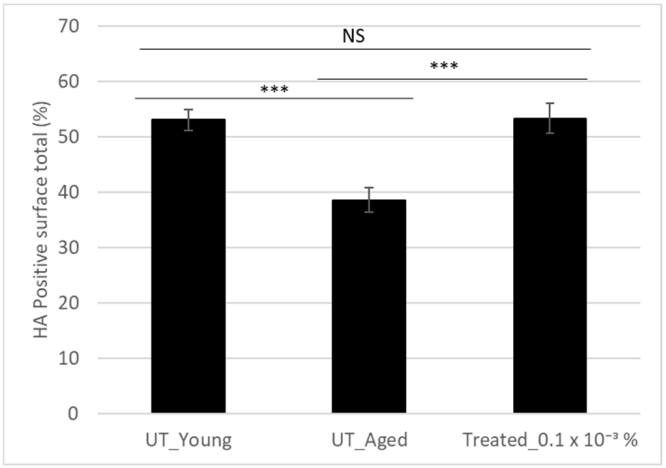

(**e**)

Figure 8. Immuno-histological analysis of 3D reconstructed skins via image automated quantification analysis of (**a**) Ki67, (**b**) filaggrin, (**c**) loricrin, (**d**) collagen-7 (COL VII), and (**e**) hyaluronic acid (HA). *** $p < 0.001$, ** $p < 0.01$, * $p < 0.05$, NS: non-significant, UT: untreated. There were 3 experimental replicates and 3 image acquisition replicates for each marker; thus, 9 images were quantified per experimental condition.

Compared with the young untreated model, the expression levels of the three main cutaneous markers of the skin barrier—Ki67, loricrin, and filaggrin—were significantly decreased in the aged untreated model by −34%, −33%, and −81%, respectively. Compared with the young untreated model, COL VII, and HA were also significantly decreased in the aged untreated model by −96% and −27%, respectively. These results were expected and validate the experiment (Figure 8).

Compared with the aged untreated control, the treatment with 0.1×10^{-3}% of *Willaertia* lysate resulted in a significant increase in Ki67, filaggrin, loricrin, COL VII, and HA by +68%, +361%, +48%, +7170%, and +38%, respectively, in the 3D reconstructed aged skin model. The expression level of these cutaneous markers returned to a similar level to that of the untreated young skin model, except for COL VII, which increased significantly by 64% (Figure 8).

3.5. Extrinsic Aging Study

The objective of this investigation was to evaluate the effects of *Willaertia* lysate on different specific cutaneous markers in 3D UV-irradiated reconstructed young skin using immuno-histological techniques.

3.5.1. Histological Analysis of 3D Unirradiated Untreated Young Skin vs. 3D Irradiated Untreated and Irradiated Treated Young Skins

The global structure of the UVB-exposed reconstructed skin was consistent at both the epidermal and dermal levels, showing a pluristratified epidermis that was well differentiated from the basal layer to the *stratum corneum* and well anchored on top of the dermal equivalent filled with fibroblasts and a neosynthesized ECM. The DEJ seemed cohesive and regular (Figure 9a). However, compared with the unexposed condition, UVB stress had an impact on both the dermal and epidermal compartments. The extracellular matrix was less dense and abundant and was disorganized, impacting tissue elasticity and hydration. The extracellular matrix was also disorganized. The epidermal thickness decreased with fewer layers of living cells, impacting barrier function (Figure 9b). Compared with the untreated and UVB-exposed condition, the treatment with *Willaertia* lysate diluted at 0.2×10^{-3}% (1.6×10^{-5}% dry weight) improved ECM quality and abundance. Moreover, the treatment induced an increase in epidermal thickness (Figure 9c).

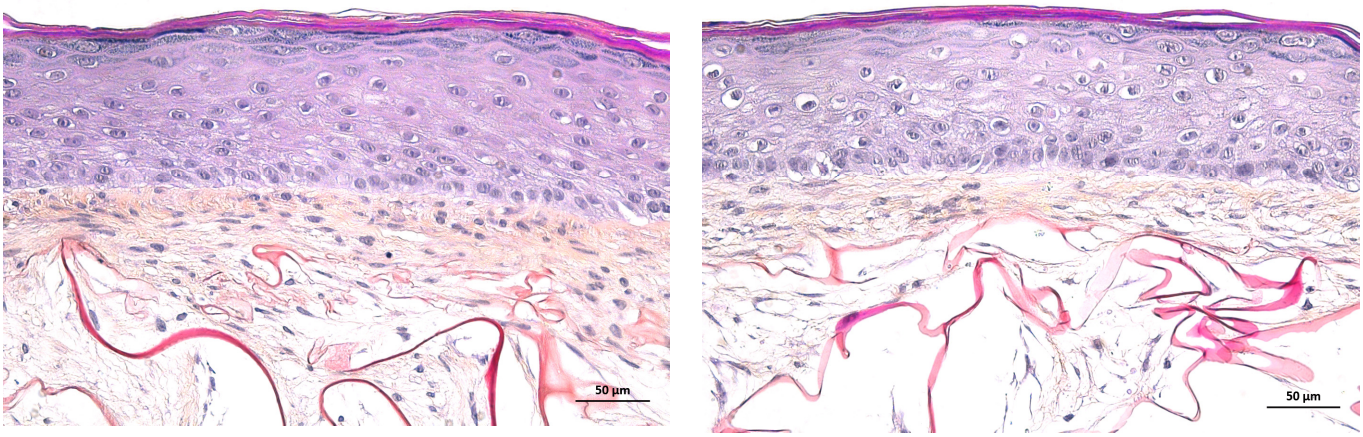

(**a**) (**b**)

Figure 9. *Cont.*

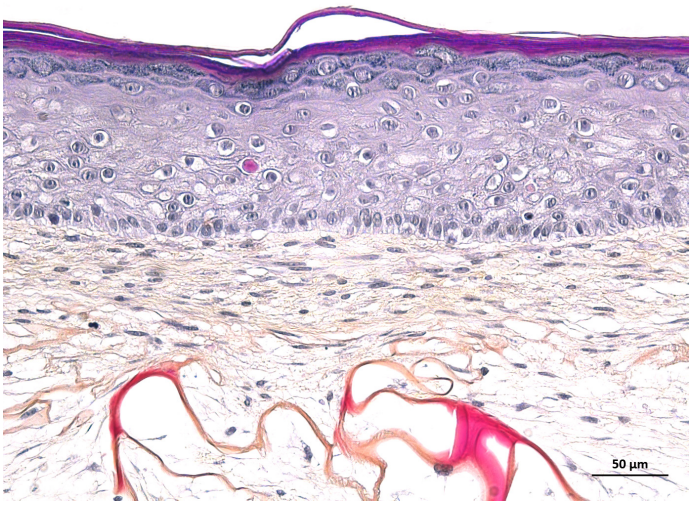

(**c**)

Figure 9. Histological analysis of 3D reconstructed skins: (**a**) untreated unirradiated young skin, (**b**) untreated irradiated young skin, and (**c**) irradiated young skin treated with *Willaertia* lysate diluted at 0.2×10^{-3}%.

3.5.2. Immuno-Histological Analysis of Specific Markers in 3D Unirradiated Untreated Young Skin vs. 3D Irradiated Untreated and Irradiated Treated Young Skins

To gain a deeper understanding of these effects, further investigations were carried out to decipher more precisely the cellular mechanisms underlying the effects of *Willaertia* lysate on the epidermis with filaggrin (Figure 10a) and loricrin (Figure 10b) as the markers; on the DEJ with laminin-332 (Figure 10c) and COL VII (Figure 10d) as the markers; and on the dermis with HA (Figure 10e), collagen-1 (COL I) (Figure 10f), and elastin (Figure 10g) as the markers.

Compared with the untreated and unirradiated control, significant decreases in filaggrin, loricrin, laminin-332, COL VII, total HA, COLI, and elastin expression by −56%, −19%, −12%, −30%, −17%, −14%, and −19%, respectively, were observed after UVB irradiation. These results were expected. Compared with the untreated and UVB-irradiated control, significant increases in filaggrin, loricrin, laminin-332, COL VII, HA, COLI, and elastin expression by +57%, +27%, +28%, +32%, +31%, +28%, and +69%, respectively, were observed with the addition of the *Willaertia* lysate treatment diluted at 0.2×10^{-3}% (Figure 10).

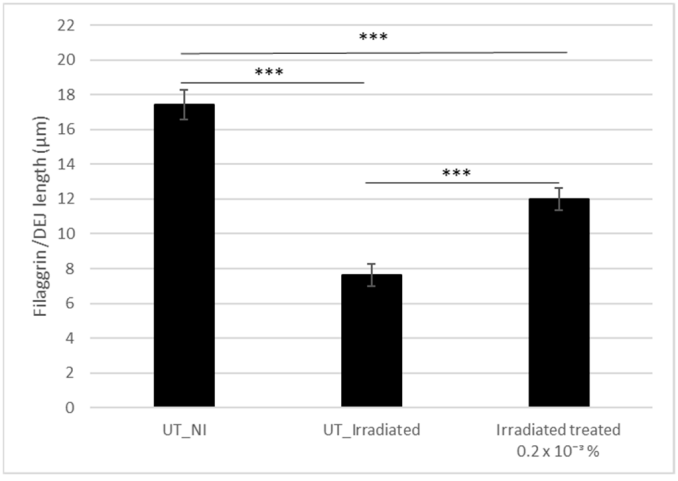

(**a**)

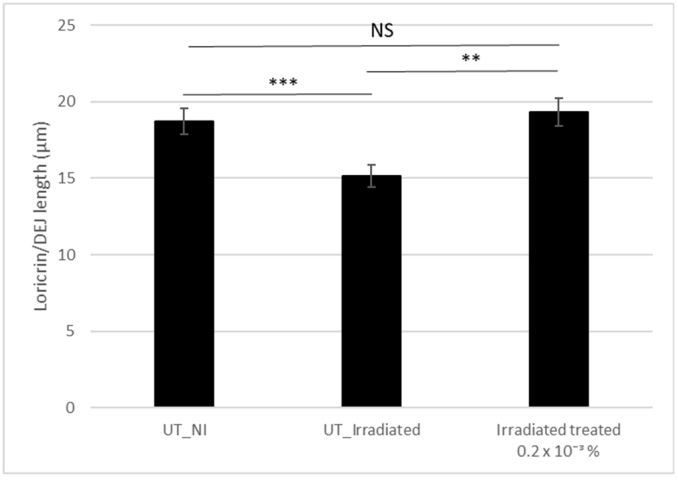

(**b**)

Figure 10. *Cont.*

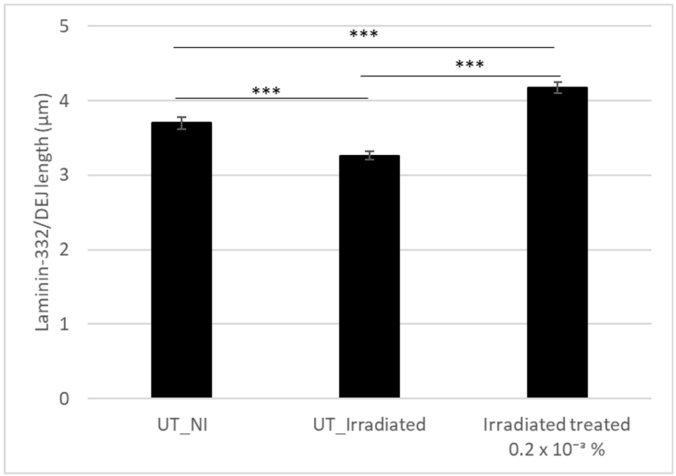

(**c**)

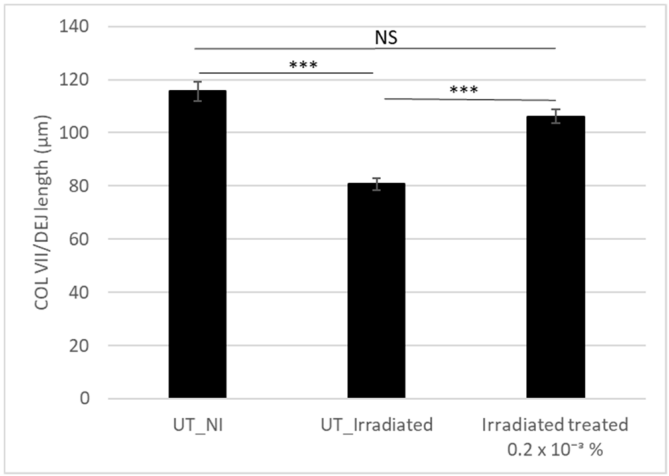

(**d**)

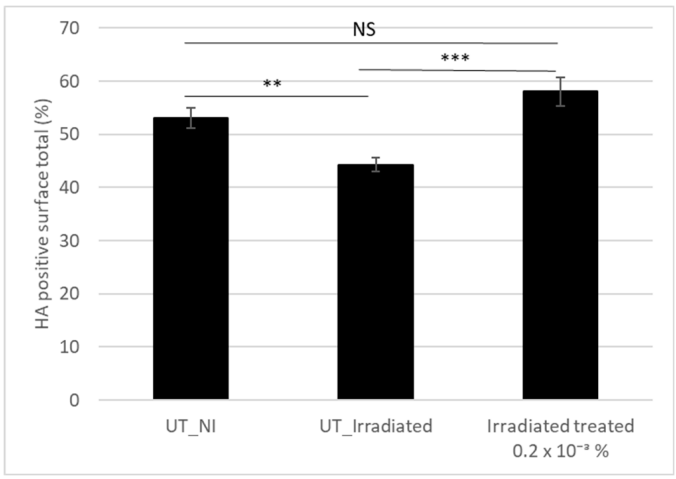

(**e**)

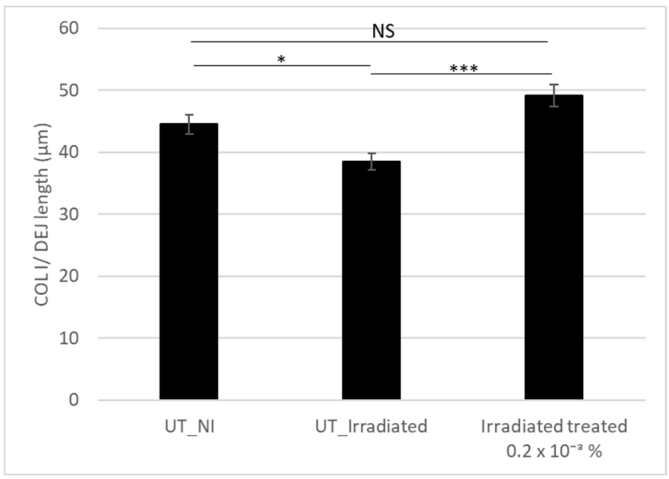

(**f**)

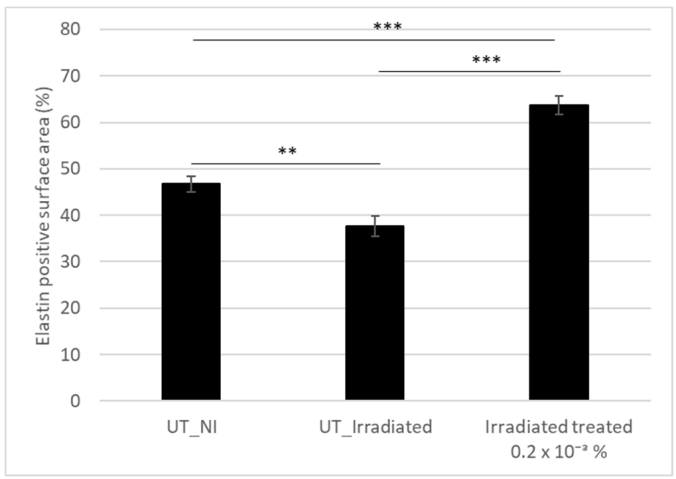

(**g**)

Figure 10. Immuno-histological analysis of 3D reconstructed young skins through image automated quantification analysis of: (**a**) filaggrin, (**b**) loricrin, (**c**) laminin-332, (**d**) COL VII, (**e**) hyaluronic acid (HA), (**f**) COL I, and (**g**) elastin. *** $p < 0.001$; ** $p < 0.01$; * $p < 0.05$; NS: non-significant; UT: untreated; NI: unirradiated. There were 3 experimental replicates and 3 image acquisition replicates for each marker; thus, 9 images were quantified per experimental condition.

It is interesting to note that the expression level of loricrin, COL VII, HA, and COL I returned to a similar level as that of the untreated and unirradiated control, and that the expression level of laminin-332 and elastin increased significantly by +13% and +36%, respectively.

Finally, considering UV exposure, the level of oxidative stress was also evaluated by determining the level of lipid peroxidation via malondialdehyde (MDA) measure (Figure 11a) and protein carbonylation (Figure 11b). Compared with the untreated and unirradiated control, a significant increase of +682% and +26% in MDA and protein carbonylation expression, respectively, was measured after UVB irradiation of the untreated young skin. Compared with the untreated and UVB irradiated control, a significant decrease of −86% and −25% in MDA and protein carbonylation expression, respectively, was observed with the addition of the *Willaertia* lysate treatment diluted at 0.2×10^{-3}%. The level of MDA expression after treatment with *Willaertia* lysate was similar to that of the untreated and unirradiated control, while protein carbonylation decreased significantly by 5%.

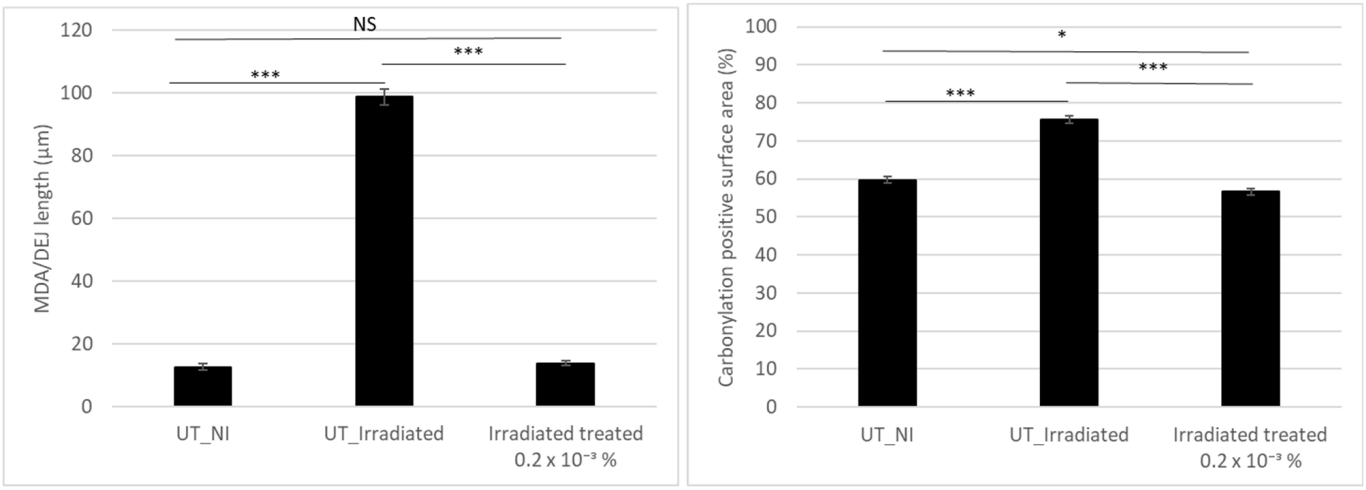

(**a**) (**b**)

Figure 11. Immuno-histological analysis of 3D reconstructed young skins through image automated quantification analysis of (**a**) MDA and (**b**) carbonylation. *** $p < 0.001$; * $p < 0.05$; NS: non-significant; UT: untreated; NI: unirradiated. There were 3 experimental replicates and 3 image acquisition replicates for each marker; thus, 9 images were quantified per experimental condition.

An additional in vitro test was conducted to evaluate the antioxidative properties of *Willaertia* lysate. Strong activity was observed at 15 mg/mL dry weight with 83% inhibition, and the IC_{50} was determined to correspond to a concentration of 8.02 mg/mL. In comparison, *Moringa oleifera* seed oil, known for its antioxidant properties [54] has an IC_{50} of 121.9 mg/mL, and thus fifteen less fold efficient than *Willaertia* lysate.

To conclude, we demonstrated that treatment of the 3D reconstructed skin model exposed to UVB with *Willaertia* lysate improved the quality and abundance of the ECM and increased the epidermal thickness. By stimulating epidermal markers such as loricrin and filaggrin, the *Willaertia* lysate treatment demonstrated its protective effects on the skin barrier; by stimulating DEJ markers such as COL VII and laminin-332, and dermal markers such as COL I, elastin, and hyaluronic acid, the *Willaertia* lysate treatment demonstrated its efficacy in improving skin firmness, elasticity, architecture, and hydration.

Moreover, the antioxidant activity of the *Willaertia* lysate treatment was demonstrated through an efficient reduction in the quantity of DPPH radicals and its efficacy in reducing oxidative stress after UV exposure was shown by the decreases in exposome markers such as protein carbonylation and lipid peroxidation expression. This complete set of coherent results demonstrated the global protective efficacy of *Willaertia* lysate against the effects of photoaging.

4. Discussion

Thermal spring waters have long been revered for their medicinal and wellness properties, showing benefits in treating a variety of conditions related to rheumatology, gastroenterology, pulmonology, and dermatology. To date, twelve samples of thermal spring water have been recognized to have potential as active ingredients in cosmetic formulations [55,56]. To the best of our knowledge, this is the first study to investigate an ingredient sourced from the thermal spring waters of Aix-les-Bains. These thermal spring waters are unique because of their origin from two different boreholes: Chevalley and Reine Hortense. The Chevalley borehole reaches a depth of 2200 m with a temperature of 71 °C, while the Reine Hortense borehole extends to 1100 m with a temperature of 38 °C. Although nearly identical in composition, the waters from these two boreholes were blended, with 36% sourced from Reine-Hortense and 34% from Chevalley. Since Roman times, the thermal spring waters of Aix les Bains have been renowned for their richness in trace elements, including calcium bicarbonate, sulfate, and sulfur. These mineral-rich waters are recognized for their therapeutic virtues, particularly in alleviating and treating rheumatic, respiratory, dermatological and circulatory conditions [57,58]. However, the mineral composition of these waters alone does not fully explain their positive effects on atopic skin. Therefore, it is worth exploring the interactions between the biological components of thermal waters and the skin, an area that has been relatively under-researched.

The living microbiota present in thermal spring waters, referred to as "hydrobiome", is increasingly recognized for its therapeutic effects on skin health. The bioactive compounds extracted from the hydrobiome help prevent skin aging by enhancing protection against UV exposure, strengthening the skin barrier function, maintaining homeostasis of skin defenses, repairing damaged skin, promoting wound healing, and reducing uneven skin pigmentation [59]. *Willaertia* lysate demonstrates all of these properties. In this study, it was demonstrated to promote cell migration in primary cultures of human dermal fibroblasts and keratinocytes, decrease the tyrosinase activity and melanin content of murine melanoma cells, and improve the quality and abundance of the extracellular matrix in aged skins to a similar level as that in young skins by stimulating epidermal markers such as Ki67, loricrin, and filaggrin, dermo-epidermal junction markers such as COLVII, and dermal markers such as hyaluronic acid. Hyaluronic acid (HA) is known to play a key role during the aging process by maintaining skin moisture. Treatment of cultured cells with *Willaertia* lysate induced a 1.8-fold increase in the expression of HAS gene responsible for HA synthesis at a dilution of 0.2%, corresponding to 1.6×10^{-2}% dry weight of the active substance. Comparatively, retinol at 0.1% can induce a six-fold increase in HAS gene expression [60]. The expression stimulation with *Willaertia* lysate was confirmed by a significant increase of 38% in HA content in the 3D aged skin model treated with 0.1×10^{-3}% of lysate, corresponding to the 9.2×10^{-5}% dry weight of the active substance, compared with the untreated aged skin. The HA content of the treated aged skin was not significantly different from that of the young skin. Therefore, even if the gene stimulation by *Willaertia* lysate is less efficient than retinol, it is sufficient to restore the skin's properties, and the *Willaertia* lysate concentration used is ten-fold lower than the retinol concentration to obtain a similar result. Finally, based on the provided evidence, *Willaertia* lysate appears to promote cell migration by creating a favorable environment for cell movement through extracellular matrix (ECM) remodeling. The lysate's ability to improve the quality and abundance of the ECM in the 3D skin model suggests that it can create a more favorable environment for cell migration.

In the case of the reconstructed young skin exposed to UVB, we demonstrated that the *Willaertia* lysate treatment improved the quality and abundance of the extracellular matrix, and increased the epidermal thickness. By stimulating epidermal markers such as loricrin and filaggrin, the *Willaertia* lysate treatment demonstrated its protective effects on the skin barrier; by stimulating dermo-epidermal junction markers, such as COLVII and laminin-332, and dermal markers, such as COL I, elastin, and HA, the *Willaertia* lysate treatment demonstrated its efficacy in improving skin firmness, elasticity, architecture, and

hydration. Moreover, the efficacy of this treatment in reducing oxidative stress after UV exposure was shown by the decreases in the levels of exposome markers such as protein carbonylation and lipid peroxidation. The exposome is a concept encompassing the totality of exposures to environmental factors, i.e., non-genetic factors, that a human organism undergoes from conception to the end of its life. Thus, the reduction in DPPH radicals and markers of oxidative damage (protein carbonylation and lipid peroxidation) indicates that *Willaertia* lysate possesses direct antioxidant properties.

This complete set of coherent results demonstrated the global protective efficacy of *Willaertia* lysate against the effects of (photo)aging and its potential for well-aging and longevity. The next step will consist of conducting a clinical study to confirm the benefits of *Willaertia* lysate for human skin care.

5. Conclusions

This is the first study to report the potential application of a non-viable form of *Willaertia magna* C2c Maky (lysate) in the field of cosmetics as a natural and biosourced postbiotic active ingredient. Significant statistical results may be partly due to natural biological variations; however, the diverse models used and the various experiments conducted all show the same trend toward efficiency. Our study's findings on the anti-aging effects of *Willaertia* lysate, a postbiotic isolated from French Alps thermal spring waters, may offer a partial explanation for the broader skin benefits attributed to thermal waters. The positive outcomes observed in our research suggest that the unique components and properties of these natural waters, including potential microbial contributions, could contribute to the therapeutic effects reported in historical and contemporary studies.

Author Contributions: Conceptualization, S.T.; methodology, M.D.S., J.R., K.L., M.B., A.S., A.C. and H.O.-P.; formal analysis, M.D.S., J.R., M.B., B.Q. and H.O.-P.; writing—original draft preparation, S.T.; writing—review and editing, M.D.S. and H.O.-P.; supervision, S.T. All authors have read and agreed to the published version of the manuscript.

Funding: This research received no external funding. The company Amoéba supported all expenses.

Institutional Review Board Statement: Not applicable.

Informed Consent Statement: Not applicable.

Data Availability Statement: The raw data supporting the conclusions of this study will be made available by the authors upon request.

Acknowledgments: The authors are very grateful to the production department of Amoéba for the *Willaertia* lysate production.

Conflicts of Interest: Authors Morgan Dos Santos, Julie Rorteau and Kilian Laho were employed by the company LabSkin Creations; LabSkin Creations, Lyon, France. Hanan Osman-Ponchet and Manon Barthe were employed by the company Laboratoires PKDERM; Laboratoires PKDERM, Grasse, France. The remaining authors were employed by the company Amoéba; Amoéba, Chassieu, France. The authors declare the funders had no role in the design of the study; in the collection, analyses, or interpretation of data; in the writing of the manuscript; or in the decision to publish the results.

References

1. Gilchrest, B.A. *Skin and Aging Processes*; CRC Press: Boca Raton, FL, USA, 1984; ISBN 978-0-8493-5472-4.
2. Kligman, A.M. Early Destructive Effect of Sunlight on Human Skin. *JAMA* **1969**, *210*, 2377–2380. [CrossRef] [PubMed]
3. Martin, K.I.; Glaser, D.A. Cosmeceuticals: The New Medicine of Beauty. *Mo. Med.* **2011**, *108*, 60–63. [PubMed]
4. Dhaliwal, S.; Rybak, I.; Ellis, S.R.; Notay, M.; Trivedi, M.; Burney, W.; Vaughn, A.R.; Nguyen, M.; Reiter, P.; Bosanac, S.; et al. Prospective, Randomized, Double-Blind Assessment of Topical Bakuchiol and Retinol for Facial Photoageing. *Br. J. Dermatol.* **2019**, *180*, 289–296. [CrossRef] [PubMed]
5. Fathalla, Z.; Shoman, M.E.; Barakat, H.S.; Al Fatease, A.; Alamri, A.H.; Abdelkader, H. Cyclodextrins and Amino Acids Enhance Solubility and Tolerability of Retinoic Acid/Tretinoin: Molecular Docking, Physicochemical, Cytotoxicity, Scratch Assay, and Topical Gel Formulations Investigation. *Pharmaceutics* **2024**, *16*, 853. [CrossRef]

6. Chaudhuri, R.K.; Bojanowski, K. Bakuchiol: A Retinol-like Functional Compound Revealed by Gene Expression Profiling and Clinically Proven to Have Anti-Aging Effects. *Int. J. Cosmet. Sci.* **2014**, *36*, 221–230. [CrossRef]
7. Malinauskiene, L.; Linauskiene, K.; Černiauskas, K.; Chomičiene, A. Bakuchiol-A New Allergen in Cosmetics. *Contact Dermat.* **2019**, *80*, 398–399. [CrossRef]
8. Gibielle, C.; Bousseksou, L.; Guéhenneux, S.; Vié, K. In a Preliminary Study on Human Subjects, a Cosmetic Cream Containing a Harungana Madagascariensis Plant Extract Induces Similar Anti-Aging Effects to a Retinol-Containing Cream. *Clin. Cosmet. Investig. Dermatol.* **2023**, *16*, 1051–1058. [CrossRef]
9. Gupta, P.L.; Rajput, M.; Oza, T.; Trivedi, U.; Sanghvi, G. Eminence of Microbial Products in Cosmetic Industry. *Nat. Prod. Bioprospect.* **2019**, *9*, 267–278. [CrossRef]
10. Janjetovic, Z.; Slominski, A.T. Promising Functions of Novel Vitamin D Derivatives as Cosmetics: A New Fountain of Youth in Skin Aging and Skin Protection. *Cosmetics* **2024**, *11*, 37. [CrossRef]
11. Luangpraditkun, K.; Pimjuk, P.; Phimnuan, P.; Wisanwattana, W.; Wisespongpand, C.; Waranuch, N.; Viyoch, J. Anti-Aging Properties of Cannabis Sativa Leaf Extract against UVA Irradiation. *Cosmetics* **2024**, *11*, 45. [CrossRef]
12. Gavrilescu, M.; Chisti, Y. Biotechnology—A Sustainable Alternative for Chemical Industry. *Biotechnol. Adv.* **2005**, *23*, 471–499. [CrossRef] [PubMed]
13. Murray, P.M.; Moane, S.; Collins, C.; Beletskaya, T.; Thomas, O.P.; Duarte, A.W.F.; Nobre, F.S.; Owoyemi, I.O.; Pagnocca, F.C.; Sette, L.D.; et al. Sustainable Production of Biologically Active Molecules of Marine Based Origin. *New Biotechnol.* **2013**, *30*, 839–850. [CrossRef] [PubMed]
14. Pérez-Rivero, C.; López-Gómez, J.P. Unlocking the Potential of Fermentation in Cosmetics: A Review. *Fermentation* **2023**, *9*, 463. [CrossRef]
15. Kim, J.; Lee, Y.I.; Mun, S.; Jeong, J.; Lee, D.-G.; Kim, M.; Jo, H.; Lee, S.; Han, K.; Lee, J.H. Efficacy and Safety of Epidermidibacterium Keratini EPI-7 Derived Postbiotics in Skin Aging: A Prospective Clinical Study. *Int. J. Mol. Sci.* **2023**, *24*, 4634. [CrossRef]
16. Duarte, M.; Oliveira, A.L.; Oliveira, C.; Pintado, M.; Amaro, A.; Madureira, A.R. Current Postbiotics in the Cosmetic Market—An Update and Development Opportunities. *Appl. Microbiol. Biotechnol.* **2022**, *106*, 5879–5891. [CrossRef]
17. Dey, R.; Mameri, M.R.; Trajkovic-Bodennec, S.; Bodennec, J.; Pernin, P. Impact of Inter-Amoebic Phagocytosis on the L. Pneumophila Growth. *FEMS Microbiol. Lett.* **2020**, *367*, fnaa147. [CrossRef]
18. Hasni, I.; Chelkha, N.; Baptiste, E.; Mameri, M.R.; Lachuer, J.; Plasson, F.; Colson, P.; La Scola, B. Investigation of Potential Pathogenicity of Willaertia Magna by Investigating the Transfer of Bacteria Pathogenicity Genes into Its Genome. *Sci. Rep.* **2019**, *9*, 18318. [CrossRef]
19. De Jonckheere, J.F.; Dive, D.G.; Pussard, M.; Vickerman, K. Willaertia Magna Gen. Nov., Sp. Nov.(Vahlkampfiidae), a Thermophilic Amoeba Found in Different Habitats. *Protistologica* **1984**, *20*, 5–13.
20. Robinson, B.S.; Christy, P.E.; De Jonckheere, J.F. A Temporary Flagellate (Mastigote) Stage in the Vahlkampfiid Amoeba Willaertia Magna and Its Possible Evolutionary Significance. *Biosystems* **1989**, *23*, 75–86. [CrossRef]
21. Fuentes-Herrera, P.B.; Herrera-Cabrera, B.E.; Martínez-Ayala, A.L.; Zamilpa, A.; Delgado-Alvarado, A. Content and Yield of L-DOPA and Bioactive Compounds of Broad Bean Plants: Antioxidant and Anti-Inflammatory Activity In Vitro. *Plants* **2023**, *12*, 3918. [CrossRef]
22. Rahman, M.M.; Islam, M.B.; Biswas, M.; Khurshid Alam, A.H.M. In Vitro Antioxidant and Free Radical Scavenging Activity of Different Parts of Tabebuia Pallida Growing in Bangladesh. *BMC Res. Notes* **2015**, *8*, 621. [CrossRef] [PubMed]
23. Brand-Williams, W.; Cuvelier, M.E.; Berset, C. Use of a Free Radical Method to Evaluate Antioxidant Activity. *LWT-Food Sci. Technol.* **1995**, *28*, 25–30. [CrossRef]
24. Germain, L.; Rouabhia, M.; Guignard, R.; Carrier, L.; Bouvard, V.; Auger, F.A. Improvement of Human Keratinocyte Isolation and Culture Using Thermolysin. *Burns* **1993**, *19*, 99–104. [CrossRef]
25. Dos Santos, M.; Metral, E.; Boher, A.; Rousselle, P.; Thepot, A.; Damour, O. In Vitro 3-D Model Based on Extending Time of Culture for Studying Chronological Epidermis Aging. *Matrix Biol.* **2015**, *47*, 85–97. [CrossRef]
26. de Oliviera Nascimento, L.; Massari, P.; Wetzler, L. The Role of TLR2 in Infection and Immunity. *Front. Immunol.* **2012**, *3*, 79. [CrossRef]
27. Khanmohammadi, S.; Rezaei, N. Role of Toll-like Receptors in the Pathogenesis of COVID-19. *J. Med. Virol.* **2021**, *93*, 2735–2739. [CrossRef]
28. Takeda, K.; Akira, S. TLR Signaling Pathways. *Semin. Immunol.* **2004**, *16*, 3–9. [CrossRef]
29. Koshak, A.E.; Algandaby, M.M.; Mujallid, M.I.; Abdel-Naim, A.B.; Alhakamy, N.A.; Fahmy, U.A.; Alfarsi, A.; Badr-Eldin, S.M.; Neamatallah, T.; Nasrullah, M.Z.; et al. Wound Healing Activity of Opuntia Ficus-Indica Fixed Oil Formulated in a Self-Nanoemulsifying Formulation. *Int. J. Nanomed.* **2021**, *16*, 3889–3905. [CrossRef]
30. Shive, C.; Pandiyan, P. Inflammation, Immune Senescence, and Dysregulated Immune Regulation in the Elderly. *Front. Aging* **2022**, *3*, 840827. [CrossRef]
31. Abbasi, S.; Sinha, S.; Labit, E.; Rosin, N.L.; Yoon, G.; Rahmani, W.; Jaffer, A.; Sharma, N.; Hagner, A.; Shah, P.; et al. Distinct Regulatory Programs Control the Latent Regenerative Potential of Dermal Fibroblasts during Wound Healing. *Cell Stem Cell* **2020**, *27*, 396–412.e6. [CrossRef]

32. Johnson, K.; Zhu, S.; Tremblay, M.S.; Payette, J.N.; Wang, J.; Bouchez, L.C.; Meeusen, S.; Althage, A.; Cho, C.Y.; Wu, X.; et al. A Stem Cell-Based Approach to Cartilage Repair. *Science* **2012**, *336*, 717–721. [CrossRef] [PubMed]
33. Umansky, K.B.; Gruenbaum-Cohen, Y.; Tsoory, M.; Feldmesser, E.; Goldenberg, D.; Brenner, O.; Groner, Y. Runx1 Transcription Factor Is Required for Myoblasts Proliferation during Muscle Regeneration. *PLoS Genet.* **2015**, *11*, e1005457. [CrossRef] [PubMed]
34. Xue, H.; Zha, M.; Tang, Y.; Zhao, J.; Du, X.; Wang, Y. Research Progress on the Extraction and Purification of Anthocyanins and Their Interactions with Proteins. *Molecules* **2024**, *29*, 2815. [CrossRef] [PubMed]
35. Zeng, A.; Li, H.; Guo, L.; Gao, X.; McKinney, S.; Wang, Y.; Yu, Z.; Park, J.; Semerad, C.; Ross, E.; et al. Prospectively Isolated Tetraspanin+ Neoblasts Are Adult Pluripotent Stem Cells Underlying Planaria Regeneration. *Cell* **2018**, *173*, 1593–1608.e20. [CrossRef]
36. Busjahn, A.; Aydin, A.; Uhlmann, R.; Krasko, C.; Bähring, S.; Szelestei, T.; Feng, Y.; Dahm, S.; Sharma, A.M.; Luft, F.C.; et al. Serum- and Glucocorticoid-Regulated Kinase (SGK1) Gene and Blood Pressure. *Hypertension* **2002**, *40*, 256–260. [CrossRef]
37. Jiang, D.; Fu, C.; Xiao, J.; Zhang, Z.; Zou, J.; Ye, Z.; Zhang, X. SGK1 Attenuates Oxidative Stress-Induced Renal Tubular Epithelial Cell Injury by Regulating Mitochondrial Function. *Oxid. Med. Cell. Longev.* **2019**, *2019*, 2013594. [CrossRef]
38. Mason, J.A.; Cockfield, J.A.; Pape, D.J.; Meissner, H.; Sokolowski, M.T.; White, T.C.; Valentín López, J.C.; Liu, J.; Liu, X.; Martínez-Reyes, I.; et al. SGK1 Signaling Promotes Glucose Metabolism and Survival in Extracellular Matrix Detached Cells. *Cell Rep.* **2021**, *34*, 108821. [CrossRef]
39. Daitoku, H.; Kaneko, Y.; Yoshimochi, K.; Matsumoto, K.; Araoi, S.; Sakamaki, J.; Takahashi, Y.; Fukamizu, A. Nontranscriptional Function of FOXO1/DAF-16 Contributes to Translesion DNA Synthesis. *Mol. Cell. Biol.* **2016**, *36*, 2755–2766. [CrossRef]
40. Dang, R.; Yang, M.; Cui, C.; Wang, C.; Zhang, W.; Geng, C.; Han, W.; Jiang, P. Activation of Angiotensin-Converting Enzyme 2/Angiotensin (1-7)/Mas Receptor Axis Triggers Autophagy and Suppresses Microglia Proinflammatory Polarization via Forkhead Box Class O1 Signaling. *Aging Cell* **2021**, *20*, e13480. [CrossRef]
41. Graves, D.T.; Milovanova, T.N. Mucosal Immunity and the FOXO1 Transcription Factors. *Front. Immunol.* **2019**, *10*, 2530. [CrossRef]
42. Link, W. Introduction to FOXO Biology. In *FOXO Transcription Factors. Methods in Molecular Biology*; Humana: New York, NY, USA, 2019; Volume 1890, pp. 1–9. [CrossRef]
43. Korsmeyer, S.J. BCL-2 Gene Family and the Regulation of Programmed Cell Death. *Cancer Res.* **1999**, *59*, 1693s–1700s. [CrossRef] [PubMed]
44. Ruvolo, P.P.; Deng, X.; May, W.S. Phosphorylation of Bcl2 and Regulation of Apoptosis. *Leukemia* **2001**, *15*, 515–522. [CrossRef] [PubMed]
45. Siddiqui, W.A.; Ahad, A.; Ahsan, H. The Mystery of BCL2 Family: Bcl-2 Proteins and Apoptosis: An Update. *Arch. Toxicol.* **2015**, *89*, 289–317. [CrossRef] [PubMed]
46. He, Z.; Mei, L.; Connell, M.; Maxwell, C.A. Hyaluronan Mediated Motility Receptor (HMMR) Encodes an Evolutionarily Conserved Homeostasis, Mitosis, and Meiosis Regulator Rather than a Hyaluronan Receptor. *Cells* **2020**, *9*, 819. [CrossRef]
47. Wang, S.; Xiong, Y.; Chen, J.; Ghanem, A.; Wang, Y.; Yang, J.; Sun, B. Three Dimensional Printing Bilayer Membrane Scaffold Promotes Wound Healing. *Front. Bioeng. Biotechnol.* **2019**, *7*, 348. [CrossRef]
48. Liu, L.; Liu, Y.; Li, J.; Du, G.; Chen, J. Microbial Production of Hyaluronic Acid: Current State, Challenges, and Perspectives. *Microb. Cell Factories* **2011**, *10*, 99. [CrossRef]
49. Siiskonen, H.; Oikari, S.; Pasonen-Seppänen, S.; Rilla, K. Hyaluronan Synthase 1: A Mysterious Enzyme with Unexpected Functions. *Front. Immunol.* **2015**, *6*, 43. [CrossRef]
50. Skandalis, S.S.; Karalis, T.; Heldin, P. Intracellular Hyaluronan: Importance for Cellular Functions. *Semin. Cancer Biol.* **2020**, *62*, 20–30. [CrossRef]
51. Claus, S.; Fischer, J.; Mégarbané, H.; Mégarbané, A.; Jobard, F.; Debret, R.; Peyrol, S.; Saker, S.; Devillers, M.; Sommer, P.; et al. A p.C217R Mutation in Fibulin-5 from Cutis Laxa Patients Is Associated with Incomplete Extracellular Matrix Formation in a Skin Equivalent Model. *J. Investig. Dermatol.* **2008**, *128*, 1442–1450. [CrossRef]
52. Halper, J.; Kjaer, M. Basic Components of Connective Tissues and Extracellular Matrix: Elastin, Fibrillin, Fibulins, Fibrinogen, Fibronectin, Laminin, Tenascins and Thrombospondins. *Adv. Exp. Med. Biol.* **2014**, *802*, 31–47. [CrossRef]
53. Papke, C.L.; Yanagisawa, H. Fibulin-4 and Fibulin-5 in Elastogenesis and beyond: Insights from Mouse and Human Studies. *Matrix Biol.* **2014**, *37*, 142–149. [CrossRef] [PubMed]
54. Athikomkulchai, S.; Tunit, P.; Tadtong, S.; Jantrawut, P.; Sommano, S.R.; Chittasupho, C. Moringa Oleifera Seed Oil Formulation Physical Stability and Chemical Constituents for Enhancing Skin Hydration and Antioxidant Activity. *Cosmetics* **2021**, *8*, 2. [CrossRef]
55. Figueiredo, A.C.; Rodrigues, M.; Mourelle, M.L.; Araujo, A.R.T.S. Thermal Spring Waters as an Active Ingredient in Cosmetic Formulations. *Cosmetics* **2023**, *10*, 27. [CrossRef]
56. Merial-Kieny, C.; Castex-Rizzi, N.; Selas, B.; Mery, S.; Guerrero, D. Avène Thermal Spring Water: An Active Component with Specific Properties. *J. Eur. Acad. Dermatol. Venereol.* **2011**, *25*, 2–5. [CrossRef] [PubMed]
57. Station Thermale d'Aix Les Bains—Thermes Chevalley | ValVital. Available online: https://www.valvital.fr/Nos-stations-thermales/Aix-les-Bains-Station-thermale-d-Aix-les-Bains (accessed on 19 August 2024).

58. Cure Thermale Rhumatologie & Voies Respiratoires à Aix-les-Bains. Available online: https://www.thermes-aixlesbains.com/ (accessed on 19 August 2024).
59. Mourelle, M.L.; Gómez, C.P.; Legido, J.L. Hydrobiome of Thermal Waters: Potential Use in Dermocosmetics. *Cosmetics* **2023**, *10*, 94. [CrossRef]
60. Li, W.-H.; Wong, H.-K.; Serrano, J.; Randhawa, M.; Kaur, S.; Southall, M.D.; Parsa, R. Topical Stabilized Retinol Treatment Induces the Expression of HAS Genes and HA Production in Human Skin in Vitro and in Vivo. *Arch. Dermatol. Res.* **2017**, *309*, 275–283. [CrossRef]